ACS OMEGA

http://pubs.acs.org/journal/acsodf

Article

# Intelligent Method to Optimize the Frequency Modulation for Beam Pumping System Based on Deep Reinforcement Learning

Ruichao Zhang,* Dechun Chen, and Liangfei Xiao

Cite This: *ACS Omega* 2023, 8, 9475−9485

Read Online

ACCESS | Metrics & More | Article Recommendations

**ABSTRACT:** A mathematical simulation model of a beam pumping system with frequency conversion control is established, considering the influence of the real-time frequency variation on the motion law of a pumping unit, the longitudinal vibration of a sucker rod string, the crankshaft torque, and the motor power. On this basis, the key links such as state space, action space, and reward function are defined by using deep reinforcement learning theory, and an intelligent model to optimize the frequency modulation for a beam pumping system based on deep reinforcement learning is constructed. The simulation and field application results show that the frequency optimization model can significantly reduce the fluctuation amplitude of the polished rod load, crankshaft torque, motor power, and input power of the system, making the operation of the pumping system more stable and energy-saving. More importantly, the model can realize the independent learning and control of the corresponding parameters without manual intervention to ensure the normal operation of the system and improve the level of information and intelligent management of oil wells.

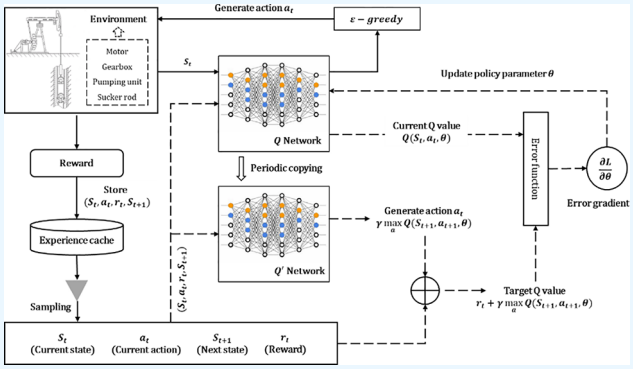


## 1. INTRODUCTION

The pumping unit is the most important artificial lifting method in most oilfields, accounting for more than 80% of the production wells.[1−3] Because of the advantages of simple structure, stable performance, and easy maintenance, beam pumping units have become the most popular pumping equipment in oilfields.[4,5] However, due to their operation characteristics, the crank shaft torque of the gearbox and the load torque of the motor fluctuate greatly, which seriously affects the operation efficiency and equipment life of the pumping system.[6] In addition, due to the large torque required for the starting of the pumping unit, it is necessary to configure a motor with larger rated power for safe starting, leading to the phenomenon of "large horse pulls small carriage", which greatly reduces the power factor and operating efficiency of the motor, and greatly wastes electric energy.[7] Therefore, in the context of global "carbon neutrality", how to improve the operation efficiency of pumping wells while maintaining production and thus reduce production energy consumption has become an urgent problem for oilfield enterprises.

In order to improve the operation efficiency of the pumping system, a lot of work has been done, mainly including the following aspects. (1) In order to improve the energy-saving effect of the motor, many new motors have been developed, which can change the mechanical characteristics of the motor and improve the motor power factor.[8,9] (2) By optimizing the four-bar linkage and balancing method, a variety of new pumping units have been developed, thus optimizing the kinematic characteristics of the polished rod and reducing the fluctuation in the net torque.[10] (3) High-efficiency components such as narrow v-belts are used to improve the transmission efficiency of the system and reduce the consumption of reactive energy.[11] Although these methods have achieved certain energy-saving effects, they cannot fundamentally solve the problem of low efficiency of the pumping system, which also makes this research a bottleneck.

In recent years, with the development of frequency modulation technology, the frequency modulation control technology of the pumping unit has been widely used in the oilfield.[12] This technology can improve the motion characteristics of the pumping system by optimizing the frequency modulation, thus reducing the fluctuation of the crank shaft torque of the gearbox and the load torque of the motor, and has a good energy-saving effect. In terms of optimizing the frequency

**Received:** December 24, 2022
**Accepted:** February 20, 2023
**Published:** March 2, 2023

modulation, relevant scholars have also done a lot of research. In 1995, Gibbs et al.[13] proposed a method of eddy current drive to perform variable speed−no stop control by combining the liquid fillage method with variable-frequency drives. In 2009, Palka and Czyz[14] determined the optimal motor-speed profile by representing the motor speed with Fourier series and searching for Fourier coefficients that maximize the production. This paper demonstrates that by changing motor speed rapidly within a single stroke, pump production can be increased while stresses in the sucker rod and motor energy consumption are reduced. In 2011, Xu et al.[15] proposed an intelligent frequency conversion control system of a beam pumping unit with an autoadapted function. The application of a frequency changer can solve the impact of the pumping unit startup load, which markedly improved the power factor. Wu et al.[16] put forward a new energy-saving method on the basis of studying the operation of beam pumping units. By adjusting the frequency of the motor, the energy consumed by the motor can be saved. In 2013, Peng and Liu[17] introduced a new technology using frequency conversion speed regulation technology to adjust stroke frequency by analyzing the past and present ways of adjusting stroke frequency. In 2014, Li et al.[18] proposed the design and implementation for the pumping unit system of Fuzzy PI controller optimized by genetic algorithms. The simulation research shows that the dynamics of speed control and fast startup performance are improved, and overshoot is suppressed effectively. In 2016, Dong et al.[19] established a mathematical model for real-time optimization of power frequency using the penalty function optimization algorithm with the root mean square of motor output power as the optimization goal. The results show that the optimized frequency model can effectively reduce the fluctuation range of polished rod load, crank shaft torque, and motor output power, and greatly save energy and consumption.

From the review of the above literature, it can be seen that the frequency conversion pumping system has a good energy-saving effect, and its optimal control is mainly based on the actual situation of the oil well, which is manually modeled and analyzed by experts to develop a one-to-one parameter optimization scheme. This method relies on refined manual work, and the workload is large, which does not meet the requirements of information and intelligent construction in oilfields. In recent years, with the continuous development of artificial intelligence technology,[20−22] deep reinforcement learning algorithms can provide a new idea for parameter optimization of frequency conversion pumping systems because of their strong self-learning ability and real-time decision-making ability.[23,24] Therefore, based on the mathematical simulation of beam pumping systems and artificial intelligence technology, this paper proposes an intelligent method to optimize the frequency modulation that does not rely on manual fine work and can self-optimize according to the actual situation of different oil wells. Through online self-learning, the method can realize the intelligent adaptive control of the frequency conversion pumping system, which is conducive to improving the dynamic performance and power saving effect of the beam pumping system.

## 2. MATERIALS AND METHODS

**2.1. Mathematical Simulation Model of the Beam Pumping System.** *2.1.1. Simulation Model of Frequency and Crank Motion.* For the frequency conversion beam pumping system, it is assumed that the power input frequency of the motor is a function $f(t)$, and the period of $f(t)$ is the same as the movement period $T$ of the polished rod. Then, the calculation model of frequency and crank motion can be obtained as shown in eq 1.

$$\begin{cases} \theta = \displaystyle\int_0^t \frac{2\pi f(t)(1-s)}{p\cdot i}\mathrm{d}t \\ \dot{\theta} = \dfrac{2\pi f(t)(1-s)}{p\cdot i} \\ \ddot{\theta} = \dfrac{2\pi f(t)(\dot{1}-s)}{p\cdot i} \end{cases} \tag{1}$$

where $\theta$ is the crank angle (rad), $\dot{\theta}$ is the crank angular velocity (rad/s), $\ddot{\theta}$ is the crank angular acceleration (rad/s$^2$), $s$ is the rotor slip of the motor, $p$ is the pole-pair numbers of the motor, and $i$ is the transmission ratio from the motor rotor to the crank.

*2.1.2. Simulation Model of Polished Rod Movement of the Pumping Unit.* Ignoring the elastic deformation of each component and the clearance of each kinematic pair, the ground device of the beam pumping system can be simplified as a four-bar linkage. Taking the bottom dead center of the polished rod as the displacement zero point and the upward direction as the positive direction of displacement, the complex vector method is applied to analyze its motion law, and then the simulation models of polished rod displacement $s_A$, polished rod velocity $v_A$, and polished rod acceleration $a_A$ can be established, as shown in eqs 2−4.

$$s_A = A(\psi_b - \psi) \tag{2}$$

$$v_A = \frac{AR}{C}\cdot\omega\cdot\frac{\sin\alpha}{\sin\beta} \tag{3}$$

$$a_A = -\frac{ARK}{CP}\cdot\omega^2\cdot\frac{\sin\beta\cos\alpha\sin\psi + \frac{R}{C}\cdot\sin\alpha\cos\beta\sin\theta_k}{(\sin\beta)^3} \tag{4}$$

where $A$ is the forearm length of the walking beam (m), $\psi$ is the angle between $C$ and $K$ (rad), $\psi_b$ is the $\psi$ angle of the polished rod at the lowest location (rad), $R$ is the crank radius (m), $C$ is the rear arm length of the walking beam (m), $\omega$ is the crank rotation angular velocity, and its value is the average of $\dot{\theta}$ in eq 1 (rad/s), $\alpha$ is the angle between the crank and the connecting rod (rad), $\beta$ is the transmission angle (rad), $K$ is the base pole length (m), $P$ is the connecting rod length (m), and $\theta_k$ is the angle between the crank and the base pole (m).

*2.1.3. Simulation Model of Longitudinal Vibration of the Sucker Rod String.* The forces on the sucker rod string of a vertical well are all longitudinal forces, including static load, inertial load, friction load, and vibration load. The force model is shown in Figure 1.

The sucker rod string is divided into several infinitesimal elements, each of which is mainly affected by gravity, viscous resistance of liquid, and elastic force. According to the force balance conditions of the elastic element and the boundary conditions of the upper and lower parts of the sucker rod string, a differential equation describing the longitudinal vibration of the sucker rod string is obtained:



https://doi.org/10.1021/acsomega.2c08170
ACS Omega 2023, 8, 9475−9485

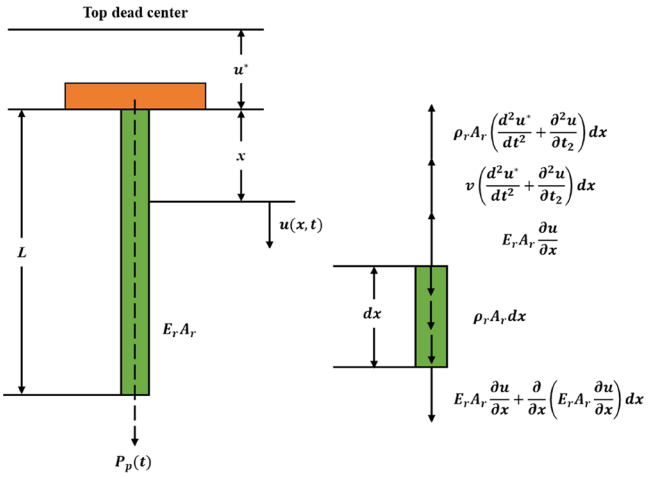


**Figure 1.** Mathematical model of longitudinal vibration of the sucker rod string.

$$\begin{cases} \dfrac{\partial^2 u}{\partial t^2} - c^2\dfrac{\partial^2 u}{\partial x^2} + v\dfrac{\partial u}{\partial t} = -\dfrac{\mathrm{d}^2 u^*(t)}{\mathrm{d}t^2} - v\dfrac{\mathrm{d}u^*(t)}{\mathrm{d}t} + g \\ u(x,t)|_{x=0} = u^*(t) \\ E_r A_r \dfrac{\partial u}{\partial x}|_{x=L} = P_p(t) \end{cases} \tag{5}$$

where $u(x, t)$ is the displacement of the section $x$ of the sucker rod string at time $t$ (m), $c$ is the propagation velocity of sound in the sucker rod string, $c = \sqrt{E_r/\rho_r}$ (m/s), $L$ is the depth of the pump (m), $g$ is the acceleration of gravity (m$^2$/s), $E_r$ is the elastic modulus of the sucker rod string (N/m$^2$), $A_r$ is the cross-sectional area of the sucker rod string (m$^2$), $u^*(t)$ is the displacement of the polished rod (m), $\rho_r$ is the density of the sucker rod string (kg/m$^3$), $v$ is the damping coefficient of downhole fluid to sucker rod string, and its calculation formula is shown in eq 8 (s$^{-1}$), and $P_p(t)$ is the liquid load of the plunger (N), which is calculated according to the static pressure difference between the suction pressure and the discharge pressure of the pump. The calculation formula is as shown in eq 6.

$$P_p(t) = A_p(p_d - p) - A_{rd}p_d + F_f \tag{6}$$

where $A_p$ is the cross-sectional area of the plunger (m$^2$), $A_{rd}$ is the cross-sectional area of the lowest sucker rod string (m$^2$), $F_f$ is the friction between the plunger and the pump barrel (N), $p_d$ is the discharge pressure of the pump (Pa), and $p$ is the pressure of liquid in the pump barrel (Pa), which changes with time and its change law is related to the opening state of the standing valve and traveling valve and the position of the plunger. The calculation formula is as shown in eq 7.

$$p = \begin{cases} \left[\dfrac{S_g}{S_g - (S_p - l_p)}\right]^n p_s & v_p < 0,\ l_p \geq l_{to} \\ p_d & v_p < 0,\ l_p \leq l_{to} \\ \left(\dfrac{S_{og}}{S_{og} + l_p}\right)^n p_d & v_p > 0,\ l_p \leq l_{so} \\ p_s & v_p > 0,\ l_p \geq l_{so} \end{cases} \tag{7}$$

where $S_g$ is the converted length of natural gas in the pump barrel when the plunger is at the top dead center (m), $S_p$ is the gas−oil ratio, $S_{og}$ is the converted length of natural gas in the pump barrel when the plunger is at the bottom dead center (m), $l_p$ is the displacement of the plunger at any time (m), $l_{to}$ is the displacement of the plunger when the traveling valve is opened (m), $l_{so}$ is the displacement of the plunger when the standing valve is opened (m), $v_p$ is the movement speed of the plunger (m/s), and $p_s$ is the suction pressure of the pump (Pa).

The calculation formula of the damping coefficient is as follows:

$$v = \frac{12\pi\mu}{\rho_r A_r}\left(\frac{D_r}{D_{ti} - D_r}\right)\left[\left(0.2 + 0.39\frac{D_r}{D_{ti}}\right) + \frac{2.197 \times 10^4}{25}\left(\frac{D_r}{D_{ti}} - 0.381\right)^{2.57} \times \frac{D_c^2 - D_r^2}{L_r D_r}\right] \tag{8}$$

where $\mu$ is the dynamic viscosity of liquid (Pa s), $L_r$ is the length of sucker rod (m), $D_r$ is the diameter of the sucker rod (mm), $D_{ti}$ is the external diameter of rod column coupling (mm), and $D_{ti}$ is the internal diameter of the oil pipe (mm).

The displacement and load of any section $x$ on the sucker rod string at time $t$ can be obtained by solving eq 5 with the finite difference method.[25−27] The polished rod load can be calculated by eq 9.

$$P_{RL} = A_r E_r \frac{\partial u}{\partial x}|_{x=0} \tag{9}$$

where $P_{RL}$ is the polished rod load (N).

*2.1.4. Simulation Model of Crankshaft Torque and Motor Power.* When the pumping unit is in variable speed drive, inertia torque will be formed due to the angular acceleration of each rotating component. Therefore, the net torque of the output shaft should be equal to the sum of the load torque, balance torque, and inertia torque, as shown in eq 10.

$$M_t = \mathrm{TF}\cdot\left(P_{RL} - B_{un} + \frac{J_y}{A^2}a_A\right) + (W_{cb}R + W_c R_c)\sin\varphi + J_q\varepsilon \tag{10}$$

where $M_t$ is the net torque of the reducer output shaft (N m), TF is the torque factor, $B_{un}$ is the unbalanced weight of the pumping unit structure (N), $J_y$ is the beam moment of inertia (kg m$^2$), $W_{cb}$ is the weight of the crank balancing blocks (N), $R$ is the center of gravity radius of the balancing blocks (m), $W_c$ is the weight of the crank (N), $R_c$ is the center of gravity radius of the crank (m), $J_q$ is the moment of inertia of the crank (kg m$^2$), and $\varepsilon$ is the angular acceleration of the crank (rad/s$^2$).



https://doi.org/10.1021/acsomega.2c08170
ACS Omega 2023, 8, 9475−9485

The torque and power of the motor output shaft are calculated by the following eqs 11 and 12, respectively:

$$M_d = \frac{M_t + (J_d - J_q)\varepsilon}{i} \tag{11}$$

$$N_d = \frac{M_d \cdot \omega \cdot i}{1000} \tag{12}$$

where $M_d$ is the torque of the motor output shaft (N m), $N_d$ is the power of the motor output shaft (kW), and $J_d$ is the moment of inertia of each rotating component equivalent to the crank shaft (kg m$^2$).

**2.2. Theory of Deep Reinforcement Learning.** *2.2.1. Reinforcement Learning and Q-Learning Algorithm.* Reinforcement learning means that agents interact with the environment through trial and error to learn the action strategy set, so as to maximize the cumulative rewards of agents' actions from the environment.[28−30] The learning process is shown in Figure 2. In

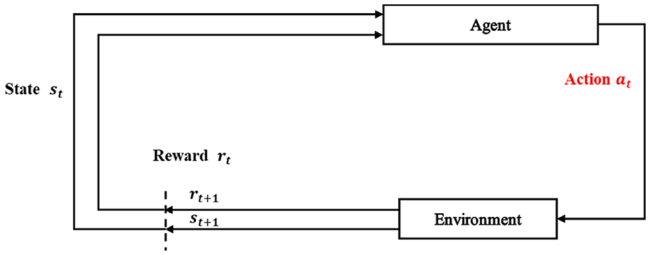


**Figure 2.** Interaction process between the agent and the environment.

essence, the interaction between the agent and the environment is a Markov decision-making process. MDP is generally represented by a quad $(S, A, R, \Pi)$, where $S$ is the state space, $A$ is the action space, and $R$ is the reward function, $\Pi$ is a policy set.

Under strategy $\Pi$, the agent executes action $a_t$ in state $s_t$, transfers to the next state $s_{t+1}$ with a certain probability, and obtains an immediate reward $r_t$. The cumulative reward is:

$$R_t = \sum_{i=t}^{T} \gamma^{i-t} r(s_i, a_i) \tag{13}$$

where $R_t$ is the cumulative reward from the state of current time $t$ to the termination state and $\gamma$ is the attenuation coefficient. The farther away from time $t$, the smaller the weight of the immediate reward.

$Q$-learning is a reinforcement learning algorithm that is not based on models but based on value functions.[31] The main idea of $Q$-learning is to define the state-action value function $Q^{\pi}(s, a)$ and learn it iteratively to obtain the optimal strategy $\pi^*(s, a)$. The $Q$ value function is as shown in eq 14.

$$Q^{\pi}(s_t, a_t) = E_{\pi}[r_t + \gamma \max_{a_{t+1}} Q^{\pi}(s_{t+1}, a_{t+1})] \tag{14}$$

*2.2.2. Deep Q-Network Algorithm.* In the traditional $Q$-learning algorithm, due to the dimension disaster, reinforcement learning is difficult to solve large-scale MDP problems or continuous space MDP problems. Therefore, the value function approximation method is proposed to solve this problem. As an algorithm with strong learning ability, deep learning can simulate the desired function by continuously learning the training set, which just makes up for the problems faced by the above reinforcement learning algorithm.[32]

The deep $Q$-learning algorithm can fit the state-action value function through deep neural network and select actions through $\varepsilon - greedy$ strategy, as shown in eq 15.

$$a = \begin{cases} \arg\max_{a \in A} Q(s, a; \omega) & \text{rand}() > \varepsilon \\ \text{Randomly select actions} & \text{rand}() < \varepsilon \end{cases} \tag{15}$$

where $\varepsilon \in (0,1)$, $\omega$ is the weight of the neural network.

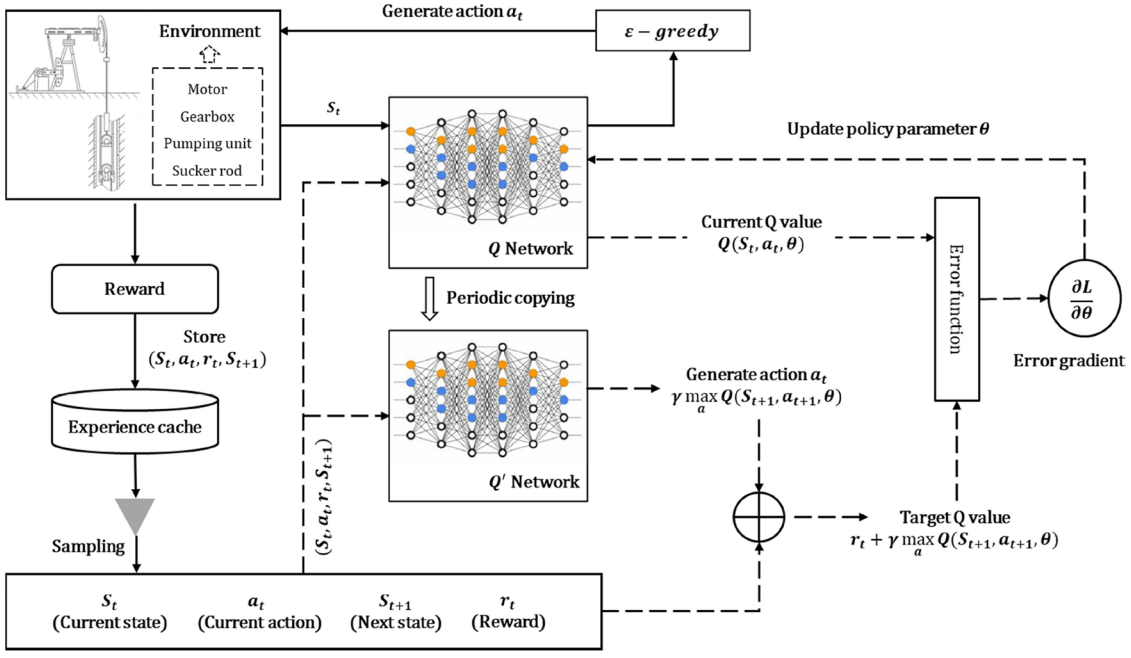


**Figure 3.** DQN model for frequency optimization.



https://doi.org/10.1021/acsomega.2c08170
ACS Omega 2023, 8, 9475−9485

In order to reduce the correlation between samples, the deep Q-network (DQN) algorithm introduces the experience playback mechanism. $\{s_t, a_t, r_t, s_{t+1}\}$ is stored in the experience pool at each training step. During training, a certain number of samples are randomly selected to update the weights of the neural network, which improves the stability of training.

In addition, in order to prevent unstable training due to the constant change of the $Q$ value when training with the same network, the DQN algorithm introduces two neural networks: target network and estimation network. At the beginning, the structure and parameters of the target network and the estimation network are the same. The estimation network is updated in real time with the training, and the target network copies the parameters of the estimation network every certain step.

Compared with traditional algorithms, the DQN algorithm does not need to model complex random problems. It uses deep neural networks to continuously train the environment transfer process $\{s_t, a_t, r_t, s_{t+1}\}$ to learn and adapt to this random rule, and when the model training is completed, the DQN algorithm can make decisions directly according to the current state, without updating all decisions every time, and can achieve real-time online optimization.

**2.3. Intelligent Optimization Model of Deep Reinforcement Learning.** *2.3.1. Structure and Framework of the Model.* The DQN algorithm of deep reinforcement learning is used to solve the problem of frequency optimization in the frequency conversion beam pumping system. The structure and framework of the frequency optimization method (DQN model) are shown in Figure 3. The structure fully shows the process of data flow and information interaction, which can be divided into data generation, caching and sampling, neural network design and calculation, gradient calculation and parameter update, and action generation and selection.

*2.3.2. Frequency Optimization Model. 2.3.2.1. State Space.* The state space is the environmental information perceived by the agent. In this method, the frequency conversion beam pumping system is defined as an agent, and the components of the frequency conversion beam pumping system together form the environment to respond to the interaction of the agent. The observable feature information provided by the environment to the agent mainly includes power supply frequency, motor net torque, motor power, gearbox net torque, and polished rod load. Therefore, the state space is represented as:

$$S = [f(t), M_{MT}(t), P_{MT}(t), M_{GB}(t), P(t)] \tag{16}$$

where $f(t)$ is the power supply frequency at time $t$ (Hz), $M_{MT}(t)$ is the output shaft torque of the motor at time $t$ (N m), $P_{MT}(t)$ is the output power of the motor at time $t$ (kW), $M_{GB}(t)$ is the output shaft torque of the gearbox at time $t$ (N m), and $P(t)$ is the polished rod load at time $t$ (kN).

*2.3.2.2. Action Space.* Action space is the relevant decision variable that needs to be optimized according to its own strategy set $\Pi$ after the agent observes the state information of the environment. For the frequency conversion beam pumping system, the decision variable is power supply frequency, so the action space is:

$$A = [f(t)] \tag{17}$$

Because the $Q$-learning algorithm cannot handle continuous actions, it is necessary to discretize the action space. According to the regulation mode of intelligent system, the characteristics of discrete actions are specified as follows:

$$f(t) = \begin{cases} \text{Increase frequency} \Delta f \\ \text{Holding frequency} \\ \text{Decrease frequency} \Delta f \end{cases} \tag{18}$$

The amount of frequency adjustment $\Delta f$ each time is a preset value, which can be determined according to the actual situation to control the smoothness of the curve.

*2.3.2.3. Reward Function.* The reward function is the quantification of task objectives, and its effective setting can provide correct guidance for the learning of agent strategies. For the variable-frequency operation of beam pumping units, the main objectives are: (1) the production capacity of the reservoir can be fully utilized, (2) the utilization rate of equipment is high and safe production is guaranteed, (3) it has high system efficiency and economic benefits. Therefore, the reward function of the model is designed as the sum of the following three reward functions.

① Design of reward function $r1$ based on the discharge coefficient.

The discharge coefficient is the ratio of the actual discharge to the theoretical discharge of the pump. For the frequency conversion beam pumping system, the larger the discharge coefficient, the better, but not too large, which indicates that the theoretical discharge of the pump selected for the well is unreasonable. Therefore, the reward function $r1$ can be designed as:

$$r1 = \begin{cases} 100(1 - e^{-20(\alpha - [\alpha]_{min})}) \ ([\alpha]_{min} \le \alpha \le [\alpha]_{max}) \\ -100 \ (\alpha < [\alpha]_{min} \text{ or } \alpha > [\alpha]_{max}) \end{cases} \tag{19}$$

where $[\alpha]_{min}$ is the minimum discharge coefficient, which is obtained when the motor rotates at a constant speed, and $[\alpha]_{max}$ is the maximum discharge coefficient, taking the maximum discharge coefficient of the actual situation in the oilfield.

② Design of reward function $r2$ based on equipment utilization.

Considering the utilization and fluctuation amplitude of various indicators of the equipment, four evaluation indexes are defined in this paper, namely, polished rod load utilization ratio $\alpha_P$, crank torque utilization ratio $\alpha_C$, sucker rod string stress utilization ratio $\alpha_R$, and motor power utilization ratio $\alpha_M$. The calculation formula is shown in eqs 20−23.

$$\alpha_P = \frac{P_{max}}{[P_{max}]} \cdot \frac{P_{max} - P_{min}}{[P_{max}]} \tag{20}$$

$$\alpha_C = \frac{M_{max}}{[M_{max}]} \cdot \frac{M_{max} - M_{min}}{[M_{max}]} \tag{21}$$

$$\alpha_R = \max(\overline{PL_i})[\max(\overline{PL_i}) - \min(\overline{PL_i})] \ i = 1, 2, \overset{***}{,} n \tag{22}$$

$$\alpha_M = \frac{P_M}{P_R} \tag{23}$$

where $[P_{max}]$ is the maximum load allowed for the polished rod of the pumping unit (kN), $P_{max}$ is the maximum load of the polished rod (kN), $P_{min}$ is the minimum load of the polished rod (kN), $[M_{max}]$ is the maximum torque allowed for the gearbox crank shaft (kN m), $M_{max}$ is the actual maximum output torque



https://doi.org/10.1021/acsomega.2c08170
ACS Omega 2023, 8, 9475−9485

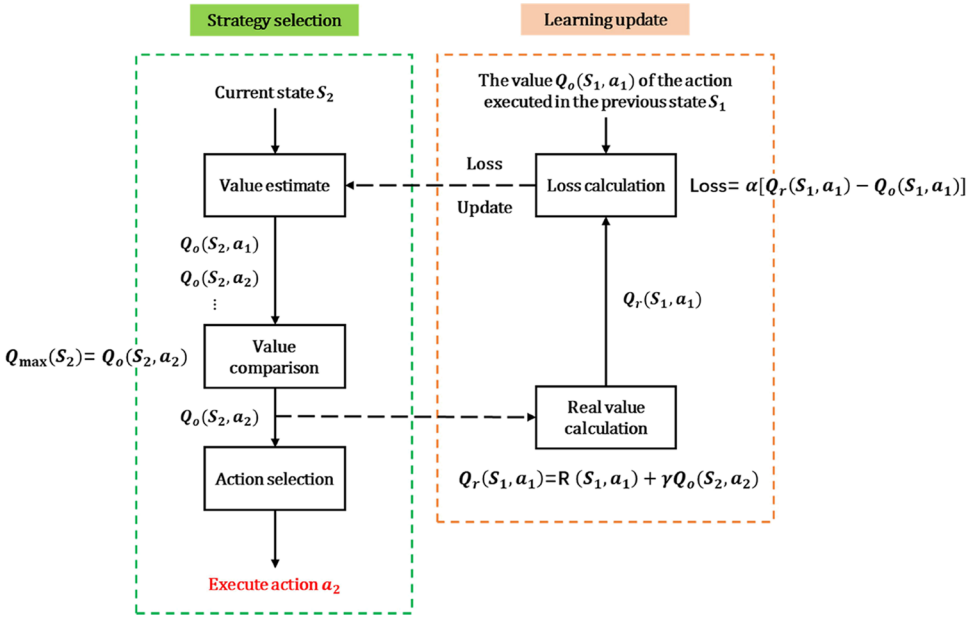


**Figure 4.** Working principle of the DQN neural network.

of the gearbox crank shaft (kN m), $M_{min}$ is the actual minimum output torque of the gearbox crank shaft (kN m), $\overline{PL_i}$ is the stress range ratio of each stage of sucker rod string, $\overline{PL_i} = \frac{[\sigma_{max}]_i - [\sigma_{min}]_i}{[\sigma_{all}]_i - [\sigma_{min}]_i}$, $i$ is the number of stages of the sucker rod, $[\sigma_{max}]_i$ is the actual maximum stress of the sucker rod string of the $i$ stage (Pa), $[\sigma_{min}]_i$ is the actual minimum stress of the sucker rod string of the $i$ stage (Pa), $[\sigma_{all}]_i$ is the maximum allowable stress of the sucker rod string of the $i$ stage (Pa), $P_M$ is the average input power of the motor (kW), and $P_R$ is the rated power of the motor (kW).

For frequency conversion beam pumping systems, the smaller the utilization ratio and fluctuation amplitude of polished rod load, crank torque, sucker rod string stress, and motor utilization ratio, the better the effect of frequency conversion. However, if the calculated utilization rate exceeds the set range, it indicates that the adopted frequency conversion effect becomes worse, and negative feedback should be given. Therefore, the reward function $r2$ of this part can be designed as:

$$r2 = r21 + r22 + r23 + r24 \tag{24}$$

$$r21 = \begin{cases} 100 \times e^{-30(\alpha_P - [\alpha_P]_{min})} \ ([\alpha_P]_{min} \le \alpha_P \le [\alpha_P]_{max}) \\ -100 \ (\alpha_P < [\alpha_P]_{min} \text{ or } \alpha_P > [\alpha_P]_{max}) \end{cases} \tag{25}$$

$$r22 = \begin{cases} 100 \times e^{-30(\alpha_C - [\alpha_C]_{min})} \ ([\alpha_C]_{min} \le \alpha_C \le [\alpha_C]_{max}) \\ -100 \ (\alpha_C < [\alpha_C]_{min} \text{ or } \alpha_C > [\alpha_C]_{max}) \end{cases} \tag{26}$$

$$r23 = \begin{cases} 100 \times e^{-50(\alpha_R - [\alpha_R]_{min})} \ ([\alpha_R]_{min} \le \alpha_R \le [\alpha_R]_{max}) \\ -100 \ (\alpha_R < [\alpha_R]_{min} \text{ or } \alpha_R > [\alpha_R]_{max}) \end{cases} \tag{27}$$

$$r24 = \begin{cases} 100 \times e^{-50(\alpha_M - [\alpha_M]_{min})} \ ([\alpha_M]_{min} \le \alpha_M \le [\alpha_M]_{max}) \\ -100 \ (\alpha_M < [\alpha_M]_{min} \text{ or } \alpha_M > [\alpha_M]_{max}) \end{cases} \tag{28}$$

where $[\alpha_P]_{max}$, $[\alpha_C]_{max}$, $[\alpha_R]_{max}$, and $[\alpha_M]_{max}$ are the highest index values of polished rod load, crank shaft torque, sucker rod stress utilization rate, and motor power utilization rate, respectively, while $[\alpha_P]_{min}$, $[\alpha_C]_{min}$, $[\alpha_R]_{min}$, and $[\alpha_M]_{min}$ are the lowest index values.

③ Design of reward function $r3$ based on system efficiency.

The system efficiency is the utilization rate of the input power in the beam pumping system, and is the ratio of active power to input power. The higher the system efficiency, the better the frequency conversion effect. However, the highest system efficiency is 1 and should not be lower than a certain lower limit. Therefore, the reward function $r3$ of this part can be designed as:

$$r3 = \begin{cases} 100 \times e^{-10(\eta - \eta_{min})} \ (\eta \ge \eta_{min}) \\ -100 \ (\eta < \eta_{min}) \end{cases} \tag{29}$$

where $\eta_{min}$ is the lowest system efficiency.

④ Design of penalty function $r4$ for violating constraint conditions.

This paper mainly considers to optimize the frequency when the stroke is unchanged, so the stroke before and after the frequency conversion should be equal. In order to improve the filling degree of the pump, the working mode of ″ slow on the upstroke and fast on the downstroke″ shall be adopted. In addition, when the frequency converter is working, the frequency is restricted to a certain range, not unlimited adjustment. Therefore, the penalty function $r4$ for violation of constraints can be designed as:

$$r4 = r41 + r42 + r43 \tag{30}$$

$$r41 = \begin{cases} 100 \ (f_{min} \le f \le f_{max}) \\ -100 \ (f < f_{min} \text{ or } f > f_{max}) \end{cases} \tag{31}$$



https://doi.org/10.1021/acsomega.2c08170
ACS Omega 2023, 8, 9475−9485

$$r42 = \begin{cases} 100\ (n_f = n_0) \\ -100\ (n_f \neq n_0) \end{cases} \quad (32)$$

$$r43 = \begin{cases} 100\ (0.8 \leq t_u/t_d \leq 1.2) \\ -100\ (t_u/t_d < 0.8 \text{ or } t_u/t_d > 1.2) \end{cases} \quad (33)$$

where $r41$ is the penalty term for violating the frequency constraint, $r42$ is the penalty term for violating the stroke equality constraint, $r43$ is the constraint penalty term for violating the time of upstroke and downstroke, $f_{max}$ is the maximum frequency regulated by the frequency converter (Hz), $f_{min}$ is the minimum frequency regulated by the frequency converter (Hz), $n_f$ is the stroke after frequency conversion ($min^{-1}$), $n_0$ is the stroke before frequency conversion ($min^{-1}$), $t_u$ is the time of upstroke (s), and $t_d$ is the time of downstroke (s).

The final reward value $r$ is the sum of the above four rewards, as shown in eq 34.

$$r = r1 + r2 + r3 + r4 \quad (34)$$

*2.3.3. Model Training Process.* After constructing the state space, action space, and reward function of the optimization model, a frequency optimization model based on the DQN neural network is established. The DQN neural network is mainly composed of two modules: strategy selection and learning update. Its working principle is shown in Figure 4.

Based on the above principles, strategy selection and learning update are carried out to achieve model training. The specific training process is shown in Figure 5.

## 3. RESULTS AND DISCUSSION

**3.1. Model Parameter Settings.** In order to verify the effectiveness of the frequency optimization model established in this paper, an oil well with a high filling coefficient in an oilfield is selected for simulation and analysis. The production parameters of the well are shown in Table 1.

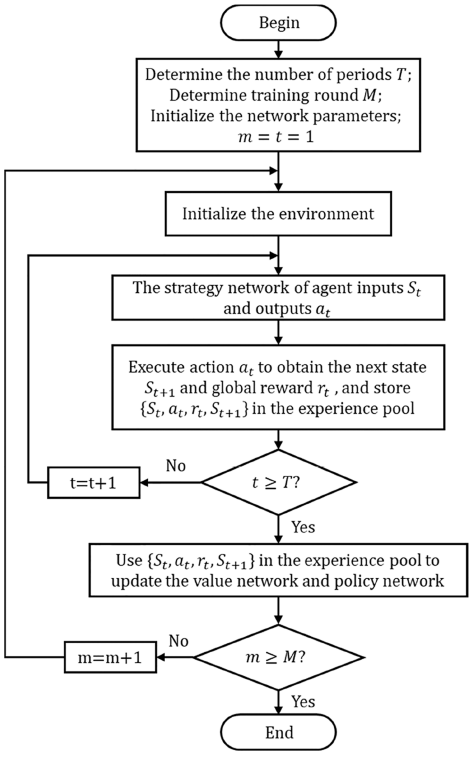


**Figure 5.** Training process of the model.

**Table 1. Production Parameters of Oil Well**

| parameter | number |
|---|---|
| pumping unit type | CYJ10-3-37HB |
| sucker rod combination | 22 mm × 738 m |
| stroke/m | 3.1 |
| fluid production/$m^3$ | 40.2 |
| pump depth/m | 738 m |
| water cut/% | 93.2 |
| oil pressure/MPa | 0.4 |
| motor type | Y280S-6 |
| pump diameter/mm | 57 |
| number of stroke/$min^{-1}$ | 6.1 |
| oil density/kg/$m^3$ | 850 |
| dynamic fluid level/m | 540 |
| gas−oil ratio/$m^3/m^3$ | 20 |
| casing pressure/MPa | 0.1 |

Based on the established reinforcement learning model, the input frequency is optimized. The optimization model uses two neural networks with the same structure. The parameters of each neural network are set as follows: the number of hidden layers is 4, the number of neural units in each hidden layer is 50, and the activation function uses the Relu function. The attenuation coefficient $\gamma$ of the algorithm is 0.96, the initial value of the learning rate $\alpha$ is 0.5, the size of the experience playback pool $D$ is 9600, and the number of randomly selected samples $m$ is 128.

**3.2. Model Training.** Model training is implemented through Python 3.8 and TensorFlow deep learning framework. The change process of model training reward value is shown in Figure 6.

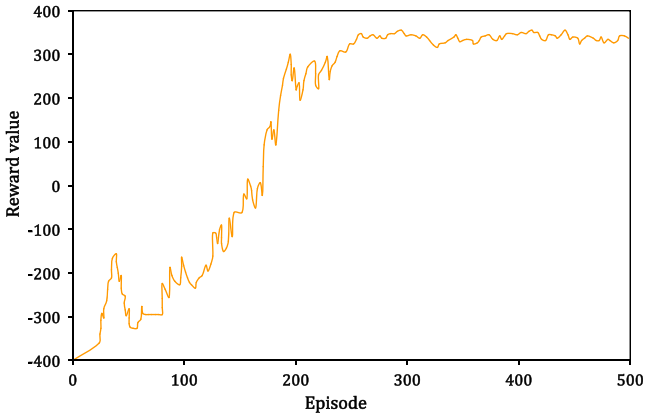


**Figure 6.** Change of reward value during learning.

According to the change of cumulative reward value in the training process, it can be seen that in the initial stage of training, the depth neural network parameters of agents are randomly initialized, and the value function cannot be correctly evaluated. At this time, the algorithm focuses on exploration, that is, try different strategies as much as possible. Therefore, the global reward value obtained by the agent at the beginning of learning has a great degree of shock. With the increase of training times, the experience pool has accumulated enough samples, the experience of agents is getting richer and richer, the value



https://doi.org/10.1021/acsomega.2c08170
ACS Omega 2023, 8, 9475−9485

function of deep neural network evaluation is getting closer to the real value, and the decision-making ability of the algorithm is constantly improving. In the late training period (Episode > 300), the agent has accumulated rich learning experience and greatly improved its decision-making ability. The algorithm is mainly used, with only a small amount of exploration reserved, and the global reward value obtained by the agent tends to be stable.

**3.3. Analysis of Optimization Results.** Using the trained reinforcement learning model to optimize the frequency, the input frequency curve within one stroke can be obtained, as shown in Figure 7.

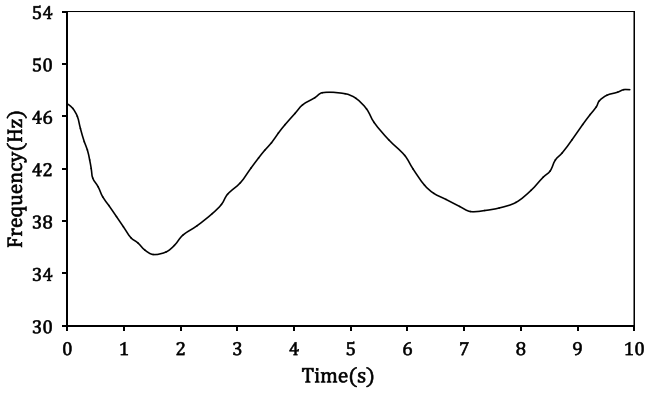


**Figure 7.** Optimized frequency curve.

The changes of polished rod load, crank torque, and motor power before and after frequency conversion are shown in Figure 891011. It can be seen that after frequency conversion, all

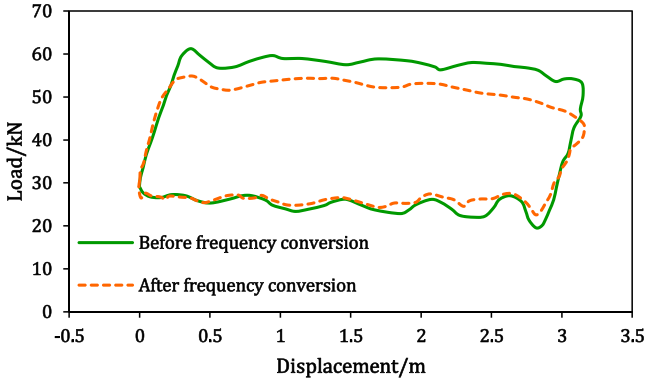


**Figure 8.** Dynamometer card before and after frequency conversion.

evaluation indexes of the system have changed significantly. Among them, the maximum load of the polished rod decreases by 11.7% and the minimum load of the polished rod increases by 12.7%, which reduces the load fluctuation amplitude of the sucker rod string and is conducive to extending the service life of the sucker rod string. The maximum net torque of the crank shaft decreases by 22.3%, basically eliminating the negative torque, reducing the fluctuation range of the crank torque, and significantly improving the torque characteristics of the pumping unit. More importantly, the fluctuation range of the motor input power curve is significantly reduced, and the average input power is reduced by 25.3%, which has obvious power saving effect. The calculation results show that the frequency

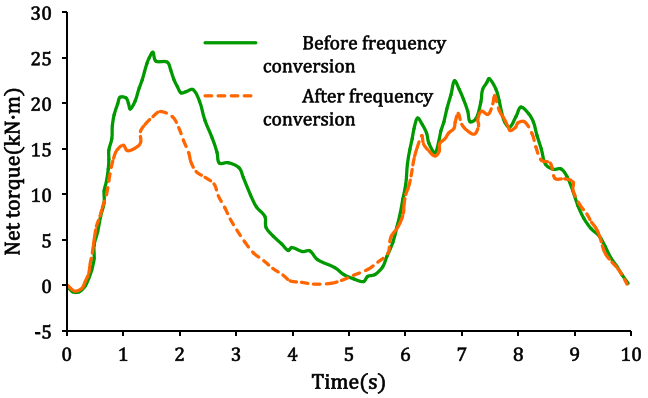


**Figure 9.** Crank net torque curve before and after frequency conversion.

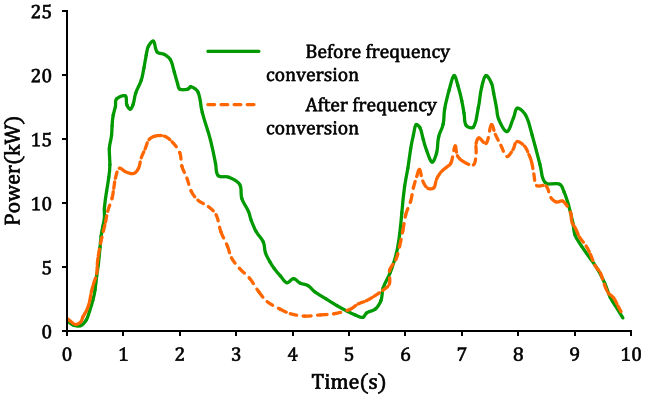


**Figure 10.** Motor power curve before and after frequency conversion.

conversion optimization technology makes the system more stable and energy-saving.

Production data of oil wells before and after frequency conversion are shown in Table 2. It can be seen that the fluid production of oil wells after frequency conversion is basically stable, the discharge coefficient and system efficiency are significantly improved, and the daily power consumption is significantly reduced. The analysis results show that the frequency conversion intelligent optimization model established in this paper can promote the stable and efficient production of oil wells, and is conducive to the intelligent and low-carbon production of oilfields.

**3.4. Field Application Effect.** Based on the optimization model, 50 oil wells in the field were applied and tested. The statistical results of field production data are shown in Table 3.

From the above data results, we can see that the frequency conversion optimization has achieved good field application effect, which is consistent with the theoretical analysis effect. After optimization, the overall performance of the pumping system has been greatly improved in which the fluctuation of crank torque and polished rod load has been reduced, and the system efficiency and pump efficiency have been greatly improved. More importantly, for oil wells with insufficient supply of formation fluid, frequency conversion optimization can effectively improve the filling degree of the pump, thus improving the fluid production and reducing production energy consumption.



https://doi.org/10.1021/acsomega.2c08170
ACS Omega 2023, 8, 9475−9485

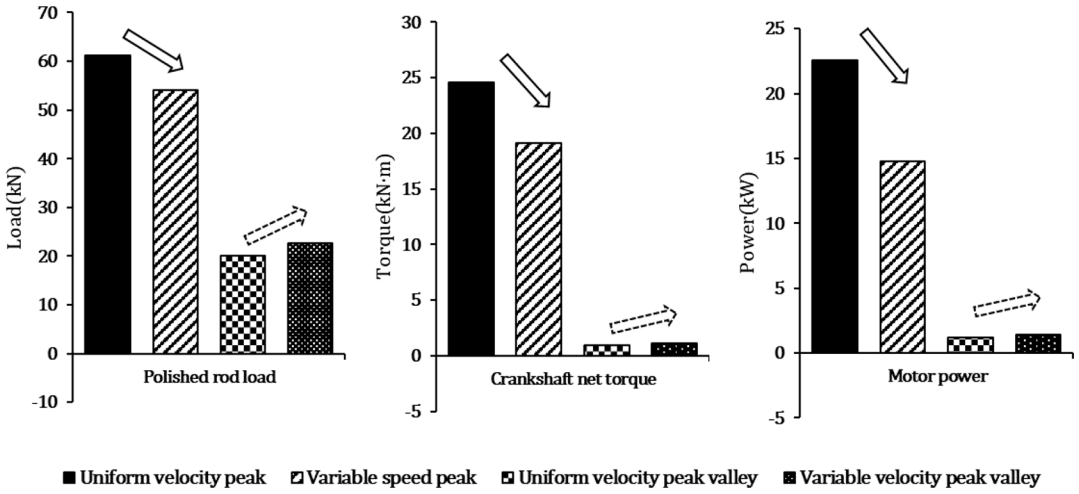


**Figure 11.** Comparison of changes in various indexes.

**Table 2. Production Data before and after Frequency Conversion**

| parameter | fluid production (t/d) | daily power consumption (kW h) |
|---|---|---|
| before frequency conversion | 40.2 | 231.2 |
| after frequency conversion | 40.7 | 181.6 |
| difference | 0.5 | 49.6 |

**Table 3. Statistical Results of Field Production Data**

| index | before optimization | after optimization | absolute difference | relative difference |
|---|---|---|---|---|
| average liquid production (t/d) | 42.1 | 46.4 | 4.3 | 10.2% |
| Average impulse times ($min^{-1}$) | 4.52 | 4.06 | −0.46 | −10.2% |
| average submergence (m) | 290.5 | 300.3 | 9.8 | 3.4% |
| average pump efficiency (%) | 48.4 | 55.8 | 7.4 | 15.3% |
| average system efficiency (%) | 18.3 | 22.6 | 4.3 | 23.5% |
| average daily power consumption (kW h) | 235.4 | 203.7 | −31.7 | −13.5% |
| average power factor of motor | 0.59 | 0.81 | 0.22 | 37.3% |
| average maximum load (kN) | 53.2 | 48.9 | −4.3 | −8.1% |
| average minimum load (kN) | 20.3 | 19.5 | −0.8 | −3.9% |

## 4. CONCLUSIONS

(1) Based on the structural characteristics and working principle of the beam pumping system with frequency conversion control, the variation laws of the suspension point movement, the force state of the sucker rod string, and the crankshaft torque and the motor power of the pumping system under frequency conversion condition are analyzed, and the mathematical simulation model of the beam pumping system is established, which provides a model basis for the optimization of the frequency.

(2) On the basis of the mathematical simulation model of the beam pumping system, the key links such as state space, action space, and reward function are defined by using the deep reinforcement learning theory, thus an intelligent model to optimize the frequency modulation for the beam pumping system based on the DQN algorithm is constructed. The simulation results show that the frequency optimization model can significantly reduce the fluctuation amplitude of polished rod load, crankshaft torque, motor power, and input power of the system, making the operation of the pumping system more stable and energy-saving. In addition, considering that the maximum value and fluctuation amplitude of the motor load torque are significantly reduced after frequency optimization, it is suggested that the installed power of the motor can be reasonably reduced to further improve the power saving effect.

(3) Deep reinforcement learning has strong intelligent decision-making ability and generalization perception ability. For the same type of beam pumping system, the deep reinforcement learning optimization model established in this paper can use the DQN algorithm which inherits the existing strategy set to train the new scene, and the training has faster convergence speed and better convergence results. Therefore, the online real-time optimization of frequency can be realized.

## AUTHOR INFORMATION

### Corresponding Author

**Ruichao Zhang** − *Shandong Institute of Petroleum and Chemical Technology, Dongying 257061, China;* orcid.org/0000-0001-7802-086X; Email: zrcupc@sdipct.edu.cn

### Authors

**Dechun Chen** − *China University of Petroleum (East China), Qingdao 266580, China*

**Liangfei Xiao** − *China University of Geosciences, Beijing 100083, China*

Complete contact information is available at: https://pubs.acs.org/10.1021/acsomega.2c08170

### Notes

The authors declare no competing financial interest.



https://doi.org/10.1021/acsomega.2c08170
ACS Omega 2023, 8, 9475−9485

## ■ ACKNOWLEDGMENTS

This research is supported by Dongying Science Development Fund (DJ2021003).

## ■ NOMENCLATURE

| | |
|---|---|
| $\theta$ | crank angle, rad |
| $\dot{\theta}$ | crank angular velocity, rad/s |
| $\ddot{\theta}$ | crank angular acceleration, rad/s$^2$ |
| $s$ | rotor slip of the motor |
| $p$ | pole-pair numbers of the motor |
| $i$ | transmission ratio from the motor rotor to the crank |
| $A$ | forearm length of walking beam, m |
| $\psi$ | angle between $C$ and $K$, rad |
| $\psi_b$ | $\psi$ angle of polished rod at the lowest location, rad |
| $R$ | crank radius, m |
| $C$ | rear arm length of walking beam, m |
| $\omega$ | crank rotation angular velocity, and its value is the average of $\dot{\theta}$, rad/s |
| $\alpha$ | angle between the crank and the connecting rod, rad |
| $\beta$ | transmission angle, rad |
| $K$ | base pole length, m |
| $P$ | connecting rod length, m |
| $\theta_k$ | angle between the crank and the base pole, m |
| $u(x, t)$ | displacement of the section $x$ of the sucker rod string at time $t$, m |
| $c$ | propagation velocity of sound in the sucker rod string, $c = \sqrt{E_r/\rho_r}$, m/s |
| $L$ | depth of the pump, m |
| $g$ | acceleration of gravity, m$^2$/s |
| $E_r$ | elastic modulus of the sucker rod string, N/m$^2$ |
| $A_r$ | cross-sectional area of the sucker rod string, m$^2$ |
| $u^*(t)$ | displacement of the polished rod, m |
| $\rho_r$ | density of the sucker rod string, kg/m$^3$ |
| $v$ | damping coefficient of downhole fluid to sucker rod string, s$^{-1}$ |
| $P_p(t)$ | liquid load of the plunger, N |
| $A_p$ | cross-sectional area of the plunger, m$^2$ |
| $A_{rd}$ | cross-sectional area of the lowest sucker rod string, m$^2$ |
| $F_f$ | friction between the plunger and the pump barrel, N |
| $p_d$ | discharge pressure of the pump, Pa |
| $p$ | pressure of liquid in the pump barrel, Pa |
| $S_g$ | converted length of natural gas in the pump barrel when the plunger is at the top dead center, m |
| $S_p$ | gas−oil ratio |
| $S_{og}$ | converted length of natural gas in the pump barrel when the plunger is at the bottom dead center, m |
| $l_p$ | displacement of plunger at any time, m |
| $l_{to}$ | displacement of plunger when the traveling valve is opened, m |
| $l_{so}$ | displacement of plunger when the standing valve is opened, m |
| $v_p$ | movement speed of the plunger, m/s |
| $p_s$ | suction pressure of the pump, Pa |
| $\mu$ | dynamic viscosity of liquid, Pa s |
| $L_r$ | length of sucker rod, m |
| $D_r$ | diameter of sucker rod, mm |
| $D_{ti}$ | external diameter of rod column coupling, mm |
| $D_{ti}$ | internal diameter of oil pipe, mm |
| $P_{RL}$ | polished rod load, N |
| $M_t$ | net torque of the reducer output shaft, N m |
| TF | torque factor |
| $B_{un}$ | unbalanced weight of pumping unit structure, N |
| $J_y$ | beam moment of inertia, kg m$^2$ |
| $W_{cb}$ | weight of the crank balancing blocks, N |
| $R$ | center of gravity radius of the balancing blocks, m |
| $W_c$ | weight of the crank, N |
| $R_c$ | center of gravity radius of the crank, m |
| $J_q$ | moment of inertia of the crank, kg m$^2$ |
| $\varepsilon$ | angular acceleration of the crank, rad/s$^2$ |
| $M_d$ | torque of motor output shaft, N m |
| $N_d$ | power of motor output shaft, kW |
| $J_d$ | moment of inertia of each rotating component equivalent to the crank shaft, kg m$^2$ |
| $R_t$ | cumulative reward from the state of current time $t$ to the termination state |
| $\gamma$ | attenuation coefficient |
| $f(t)$ | power supply frequency at time $t$, Hz |
| $M_{MT}(t)$ | output shaft torque of the motor at time $t$, N m |
| $P_{MT}(t)$ | output power of the motor at time $t$, kW |
| $M_{GB}(t)$ | output shaft torque of the gearbox at time $t$, N m |
| $P(t)$ | polished rod load at time $t$, kN |
| $[\alpha]_{min}$ | minimum discharge coefficient |
| $[\alpha]_{max}$ | maximum discharge coefficient |
| $[P_{max}]$ | maximum load allowed for the polished rod of the pumping unit, kN |
| $P_{max}$ | maximum load of the polished rod, kN |
| $P_{min}$ | minimum load of the polished rod, kN |
| $[M_{max}]$ | maximum torque allowed for the gearbox crank shaft, kN m |
| $M_{max}$ | actual maximum output torque of the gearbox crank shaft, kN m |
| $M_{min}$ | actual minimum output torque of the gearbox crank shaft, kN m |
| $\overline{PL_i}$ | stress range ratio of each stage of sucker rod string, $\overline{PL_i} = \frac{[\sigma_{max}]_i - [\sigma_{min}]_i}{[\sigma_{all}]_i - [\sigma_{min}]_i}$ |
| $i$ | number of stages of sucker rod |
| $[\sigma_{max}]_i$ | actual maximum stress of the sucker rod string of the $i$ stage, Pa |
| $[\sigma_{min}]_i$ | actual minimum stress of the sucker rod string of the $i$ stage, Pa |
| $[\sigma_{all}]_i$ | maximum allowable stress of the sucker rod string of the $i$ stage, Pa |
| $P_M$ | average input power of the motor, kW |
| $P_R$ | rated power of the motor, kW |
| $\eta_{min}$ | lowest system efficiency |
| $[\alpha_P]_{max}$ | highest index values of polished rod load |
| $[\alpha_C]_{max}$ | highest index values of crank shaft torque |
| $[\alpha_R]_{max}$ | highest index values of sucker rod stress utilization rate |
| $[\alpha_M]_{max}$ | highest index values of motor power utilization rate |
| $[\alpha_P]_{min}$ | lowest index values of polished rod load |
| $[\alpha_C]_{min}$ | lowest index values of crank shaft torque |
| $[\alpha_R]_{min}$ | lowest index values of sucker rod stress utilization rate |
| $[\alpha_M]_{min}$ | lowest index values of motor power utilization rate |
| $f_{max}$ | maximum frequency regulated by the frequency converter, Hz |
| $f_{min}$ | minimum frequency regulated by the frequency converter, Hz |
| $n_f$ | stroke after frequency conversion, min$^{-1}$ |
| $n_0$ | stroke before frequency conversion, min$^{-1}$ |
| $t_u$ | time of upstroke, s |
| $t_d$ | time of downstroke, s |



https://doi.org/10.1021/acsomega.2c08170
ACS Omega 2023, 8, 9475−9485

## REFERENCES


(1) Li, K.; Han, Y.; Wang, T. A novel prediction method for down-hole working conditions of the beam pumping unit based on 8-directions chain codes and online sequential extreme learning machine. *J. Pet. Sci. Eng.* **2018**, *160*, 285−301.

(2) Bello, O.; Dolberg, E. P.; Teodoriu, C.; Karami, H.; Devegowdva, D. Transformation of academic teaching and research: Development of a highly automated experimental sucker rod pumping unit. *J. Pet. Sci. Eng.* **2020**, *190*, No. 107087.

(3) Rowlan, O. L.; Mccoy, J. N.; Podio, A. L. Best method to balance torque loadings on a pumping unit gearbox. *J. Can. Pet. Technol.* **2015**, *44*, 27−33.

(4) Takacs, G. Exact kinematic and torsional analysis of rotaflex pumping units. *J. Pet. Sci. Eng.* **2014**, *115*, 11−16.

(5) Clarke, F.; Malone, L. Sucker rod pumping in the eagle ford shale field study. In: *SPE North America Artificial Lift Conference and Exhibition* 2016.

(6) Galeev, A. S.; Arslanov, R. I.; Suleymanov, R. N.; Filimonov, O. V. Calculation of the torque on the crank shaft of the low-speed balancing drive sucker rod pumps. *IOP Conf. Ser. Mater. Sci. Eng.* **2020**, *952*, No. 012033.

(7) Feng, Z. M.; Guo, C.; Zhang, D.; Cui, W.; Tan, C.; Xu, X.; Zhang, Y. Variable speed drive optimization model and analysis of comprehensive performance of beam pumping unit. *J. Pet. Sci. Eng.* **2020**, *191*, No. 107155.

(8) Lang, L. Problem of the beam pumping unit motor and analysis of energy-saving methods. *Energy Conservation in Petroleum and Petrochemical Industry* 2012.

(9) Feng, Z. M.; Tan, J. J.; Liu, X.; Fang, X. Selection method modelling and matching rule for rated power of prime motor used by beam pumping units. *J. Pet. Sci. Eng.* **2017**, *153*, 197−202.

(10) Zhang, C.; Wang, L.; Wu, X.; Gao, X. Performance analysis and design of a new-type wind-motor hybrid power pumping unit. *Electric Power Systems Research(Jul.)* 2022, 208.

(11) Kumaran, V. U.; Zogg, M.; Weiss, L.; Wegener, K. Design of a test stand for lifetime assessment of flat belts in power transmission. *Procedia CIRP* **2020**, *91*, 356−361.

(12) Zhu, Y. F. Application of frequency conversion technology and energy feedback control on the beam pumping unit. *Power Demand Side Management* 2013.

(13) Gibbs, S.G.; Nolen, K. B.; Morrow, F. E.; Lynch, W. E. Monitoring And Controlling Rod Pumped Wells Using Downhole Pump Cards. In: *Annual Technical Meeting*; Petroleum Society of Canada 1995.

(14) Palka, K.; Czyz, J. A. Optimizing Downhole Fluid Production of Sucker-Rod Pumps With Variable Motor Speed. *SPE Prod. Oper.* **2009**, *24*, 346−352.

(15) Xu, X.; Zhou, H.; Mao, L. Research on intelligent frequency conversion control system of pumping unit with auto-adapted function. *International Conference on Electronic and Mechanical Engineering and Information Technology, EMEIT 2011*; IEEE: Harbin, Heilongjiang, China, 12-14 August , 2011.

(16) Wu, Q.; Li, W. Y.; Xiong, H.; Rang, Y. Q.; Li, H. S.; Zhou, L. B. Study on energy saving for nodding donkey oil pump. *International Conference on Artificial Intelligence*; IEEE 2011.

(17) Peng, Y.; Liu, X. Application of Variable Frequency Speed Control to Beam Pumping Units Based on Mechanical Properties in Mechanical Controlling Engineering. *Adv. Mater. Res.* **2013**, *648*, 365−369.

(18) Li, P.; Zhang, Z. X.; Wang, C.; Zhang, Y. H. Research on Fuzzy PI Control Based on Genetic Algorithms for Beam Pumping Unit. *Proceedings of the 2014 Fourth International Conference on Instrumentation and Measurement, Computer, Communication and Control*; IEEE 2014.

(19) Dong, S. M.; Li, W. C.; Zhao, X. F.; Zhao, R. Frequency conversion beam pumping system dynamic simulation and real time frequency optimization. *China Mech. Eng.* **2016**, *27*, 1585−1590.

(20) Yao, Y.; Qiu, Y.; Cui, Y.; Wei, M.; Bai, B. Insights to surfactant huff-puff design in carbonate reservoirs based on machine learning modeling. *Chem. Eng. J.* **2023**, *451*, No. 138022.

(21) Koroteev, D.; Tekic, Z. Artificial intelligence in oil and gas upstream: trends, challenges, and scenarios for the future. *Energy AI* **2020**, *3*, No. 100041.

(22) Bello, O.; Holzmann, J.; Yaqoob, T.; Teodoriu, C. Application Of Artificial Intelligence Methods In Drilling System Design And Operations: A Review Of The State Of The Art. *De Gruyter Open (Vol.5)*; De Gruyter Open 2015.

(23) Hasselt, H. V.; Guez, A.; Silver, D. Deep reinforcement learning with double q-learning. *Comput. Sci.* **2015**, DOI: 10.48550/arXiv.1509.06461.

(24) Yao, Y.; Wei, M.; Bai, B. Descriptive statistical analysis of experimental data for wettability alteration with surfactants in carbonate reservoirs. *Fuel* **2022**, *310*, No. 122110.

(25) Cao, L. H.; Sun, J. S.; Zhang, B.; Lu, N.; Xu, Y. Q. Sensitivity analysis of the temperature profile changing law in the production string of a high-pressure high-temperature gas well considering the coupling relation among the gas flow friction, gas properties, temperature, and pressure. *Front. Phys.* **2022**, *10*, No. 1050229.

(26) Gibbs, S. G. Predicting the behavior of sucker-rod pumping systems. *J. Pet. Technol.* **1963**, *15*, 769−778.

(27) Gibbs, S. G.; Neely, A. B. Computer diagnosis of down-hole conditions in sucker rod pumping wells. *J. Pet. Technol.* **1966**, *18*, 91−98.

(28) Sutton, R. S.; Barto, A. G. Reinforcement learning: an introduction. *IEEE Trans. Neural Netw.* **1998**, *9*, 1054.

(29) Mnih, V.; Kavukcuoglu, K.; Silver, D.; Rusu, A. A.; Veness, J.; Bellemare, M. G.; Graves, A.; Riedmiller, M.; Fidjeland, A. K.; Ostrovski, G.; et al. Human-level control through deep reinforcement learning. *Nature* **2015**, *518*, 529−533.

(30) Dayan, P.; Balleine, B. W. Reward, motivation, and reinforcement learning. *Neuron* **2002**, *36*, 285−298.

(31) Watkins, C. J. C. H.; Dayan, P. Technical note: q-learning. *Mach. Learn.* **1992**, *8*, 279−292.

(32) Mousavi, S. S.; Schukat, M.; Howley, E. *Deep Reinforcement Learning: An Overview. Lecture Notes in Networks and Systems*. 2017, 426−440.




https://doi.org/10.1021/acsomega.2c08170
*ACS Omega* 2023, 8, 9475−9485